Published in final edited form as:
Invest Radiol. 2009 August ; 44(8): 454–462. doi:10.1097/RLI.0b013e3181a8b015.

Multishot Targeted PROPELLER Magnetic Resonance Imaging: *Description of the Technique and Initial Applications*

Jie Deng, PhD[1,2] and **Andrew C. Larson, PhD**[1,2,3]

[1] Department of Radiology, Northwestern University, Chicago, IL, USA

[2] Department of Biomedical Engineering, Northwestern University, Chicago, IL, USA

[3] Robert H. Lurie Comprehensive Cancer Center, Northwestern University, Chicago, IL, USA

Abstract

Objectives—To test the feasibility of combining inner-volume imaging (IVI) techniques with conventional multishot periodically rotated overlapping parallel lines with enhanced reconstruction (PROPELLER) techniques for targeted-PROPELLER magnetic resonance imaging.

Materials and Methods—Perpendicular section-selective gradients for spatially selective excitation and refocusing RF pulses were applied to limit the refocused field-of-view (FOV) along the phase-encoding direction for each rectangular blade image. We performed comparison studies in phantoms and normal volunteers by using targeted-PROPELLER methods for a wide range of imaging applications that commonly use turbo-spin-echo (TSE) approaches (brain, abdominal, vessel wall, cardiac).

Results—In these initial studies, we demonstrated the feasibility of using targeted-PROPELLER approaches to limit the imaging FOV thereby reducing the number of blades or permitting increased spatial resolution without commensurate increases in scan time. Both phantom and in vivo motion studies demonstrated the potential for more robust regional self-navigated motion correction compared with conventional full FOV PROPELLER methods.

Conclusion—We demonstrated that the reduced FOV targeted-PROPELLER technique offers the potential for reducing imaging time, increasing spatial resolution, and targeting specific areas for robust regional motion correction.

Keywords

PROPELLER; targeted; inner-volume-imaging; reduced FOV

INTRODUCTION

The multishot turbo spin echo periodically rotated overlapping parallel lines with enhanced reconstruction (TSE-PROPELLER) method[1] has recently been employed for both brain and abdominal imaging applications. PROPELLER permits T2-weighted,[2,3] T1-weighed,[2,4,5] and diffusion-weighted[6–10] image contrast whereas improving image quality by reducing sensitivity to field inhomogeneities and bulk motion.[2–4,6,7,10,11] For TSE-PROPELLER, each data segment are sampled as a rotating rectilinear strip (so-called “blade”) along a concentric propeller-shaped *k*-space trajectory. With this novel sampling pattern, oversampling of the

The corresponding author: Andrew C. Larson, Northwestern University, Department of Radiology, 737 N. Michigan Ave, Suite 1600, Chicago, IL 60611, Tel: (312) 926-3499 Fax: (312)926-5991, a-larson@northwestern.edu.

Disclosures: None of the authors had a conflict of interest

central *k*-space region and averaging of the low spatial frequencies reduce the sensitivity to motion artifacts. Additionally, low-resolution images reconstructed from individual blades can be used for selfnavigated translational and rotational motion correction. However, TSE-PROPELLER methods typically require $\pi/2$ longer acquisition times compared with conventional Two-Dimensional Fourier Transform TSE (2DFT-TSE) methods. Furthermore, the presence of a wide range of tissue motion patterns within a full FOV can make regional self-navigated motion correction quite challenging.[1]

Several techniques have been proposed to shorten imaging time for TSE-PROPELLER. Anisotropic field-of-view (FOV) PROPELLER[12] and elliptical FOV[13] techniques can tailor the FOV shape to the imaged object by varying the blade width along different angles in *k*-space. These approaches reduce the requisite number of blades to reduce overall scan times. Other approaches have included *k*-space undersampling with asymmetric blades[14] and the recently introduced TurboPROP technique[15] that acquires multiple gradient echoes between each pair of refocusing RF pulses to efficiently increase the number of *k*-space lines sampled for each blade thereby reducing the total number of blades necessary for full FOV image reconstruction.

Inner-volume imaging (IVI)[16] is a unique and straightforward technique to selectively excite a smaller FOV and avoid signal disturbance from outer FOV regions. IVI has been employed for targeted half Fourier single shot TSE (HASTE) and rapid acquisition with relaxation-enhancement (RARE) sequences[17–19] to limit the FOV to a small rectangular region-of-interest (ROI) whereas avoiding wrap-in artifacts. A reduced FOV resulted in a reduced number of requisite phase-encoding (PE) lines thus decreasing image blurring because of T2W *k*-space filtering effects along the long echo train for HASTE or RARE. Targeted-HASTE and RARE techniques have been employed for real-time free-breathing abdominal and pelvic imaging applications[17] and MR-guided percutaneous interventions[18,19] with less sensitivity to susceptibility artifacts at the needle position. More recently, IVI has also been used for single-shot multislice diffusion-weighted echo planar imaging (ie, 2D ss-rFOVDWEPI[20] and 3D ss-DWSTEPI[21]) to shorten the EPI readout by targeting the FOV to either the cervical spinal cord or a localized brain volume. These techniques reduced geometric distortions and improved spatial resolution for diffusion tensor imaging.

However, to our knowledge, IVI methods have yet to be used during multishot PROPELLER acquisitions. For PROPELLER, the number of blades (and the number of TR) required to meet full FOV Nyquist sampling criteria is proportional to the imaging matrix size over the echo train length (ie, *M*/ETL). A shorter ETL, typically between 15 and 35 echoes, is commonly used for PROPELLER sequences to moderate T2 decay and to enhance the efficacy of self-navigated phase and motion correction algorithms. For a given spatial resolution, reducing the FOV will reduce the imaging matrix *M* thereby reducing the requisite number of blades and associated imaging time. Alternatively, given a constant matrix size and adequate signal-to-noise ratio (SNR), reducing the FOV should permit increased spatial resolution without increasing the imaging time. For purposes of motion correction, a localized imaging volume may be superior to a larger FOV volume that may contain multiple tissue components moving in alternate fashions (ie, different directions, distances, and/or rotation angles). An IVI acquisition with a reduced FOV may serve to improve the accuracy of self-navigated motion correction.

The purpose of our study was to investigate the feasibility of combining IVI methods with conventional PROPELLER techniques for targeted-PROPELLER magnetic resonance imaging. In phantom and normal volunteer studies, we compared multishot targeted-PROPELLER with single shot targeted-HASTE and conventional TSE-PROPELLER

techniques to demonstrate the potential to use targeted-PROPELLER methods to shorten imaging time, increase spatial resolution, and target objects for improved motion correction.

MATERIALS AND METHODS

Targeted-PROPELLER Sequence

A pulse sequence based on the Siemens BLADE implementation of PROPELLER TSE was modified to produce the targeted-PROPELLER sequence depicted in Figure 1A. During each TR, a rectilinear *k*-space strip (ie, blade) was acquired using the TSE acquisition strategy. The PE direction of each blade was rotated about the *k*-space center (Fig. 1C). Section-selective gradients for spatially selective RF excitation were applied along the PE direction for the 90° RF pulse and along the slice select (SS) direction for the 180° refocusing RF pulses (Fig. 1B). The perpendicular orientation of these section-selective gradients limited the refocused FOV along the PE direction for each rectangular blade image. FOV size along the PE direction was controlled by adjusting the amplitude of corresponding section-selective gradient whereas the refocused slice thickness (TH) was unchanged, continuing to be dependent on the amplitude of section-selective gradient applied during 180° RF refocusing pulses. These excitation orientations rotated along with the PE direction for the acquisition of each individual *k*-space blade. As previously described,[1] the overlapping central regions within each individual blade segment were used to estimate and correct the rotational and translational motions before combination to produce final full-resolution images.

For comparison purposes, we also modified a conventional HASTE sequence to produce a targeted-HASTE sequence with excitation slice selection gradients applied in the PE direction and the excitation TH equal to the selected FOV along the PE direction. Reduction of the FOV along the PE direction permitted corresponding reduction in HASTE ETL.

For multishot TSE sequences, whether the TR time is short, the longitudinal magnetization of tissues with long T1 will not fully recover at the end of each TR. Signal saturation may result in decreased SNR. To accelerate the recovery of the longitudinal magnetization within tissues having relatively longer T1 and T2, the residual transverse magnetization at the conclusion of each TR was flipped back onto the longitudinal axis using a −90° excitation pulse (the driven-equilibrium Fourier transform [DEFT] method) as shown in Figure 1A.[22,23]

All phantom and normal volunteer studies were performed using a 1.5 T clinical magnetic resonance imaging scanner (Magnetom Espree, Siemens Medical Solutions, Erlangen, Germany).

Phantom Studies

To compare the targeted-HASTE and targeted-PROPELLER techniques, we performed a study using a Siemens quality control phantom that included resolution grids oriented along both anteriorposterior (AP) and left-right (LR) directions (marker spacing of 5, 3, 2, 1, and 0.5 mm). For comparison purposes, we used a targeted-PROPELLER sequence with a large blade width (ie, long ETL), similar to the full PE matrix size of the single-shot targeted-HASTE sequence. We acquired a targeted-HASTE image and then targeted-PROPELLER images with an increasing number of acquired blades (N_{blade}), all blades evenly distributed within the propeller-shaped *k*-space. Common imaging parameters for both sequences were: FOV = 100 × 100 mm^2, TH = 5 mm, TR/TE = 3000/32 ms, matrix = 128 × 128. For targeted-HASTE, partial-Fourier ETL = 68, bandwidth (BW) = 195 Hz/pixel. Targeted-HASTE images were acquired with PE applied along AP and LR directions separately. For targeted-PROPELLER with a large blade width, ETL = 128, BW = 400 Hz/pixel. Targeted-PROPELLER images were

reconstructed from a *k*-space sampled to minimally fulfill the Nyquist criteria (N_{blade} = 1, ETL = 128) and from the oversampled *k*-space datasets with N_{blade} of 2, 4, and 8.

Next, we created a motion phantom with a vial (diameter = 20mm) of water attached atop a balloon, which was slowly inflated and deflated by using an electronic dispensing system (Cole-Parmer Instrument Co., IL), pumping water in and out at a rate of 3200 mL/min. The space within the balloon was filled with half water and half air, and the balloon surface moved periodically with the water volume changes. Another bottle of water was placed adjacent to the moving phantom serving as a representative static object. This motion phantom study was performed to demonstrate the potential for regional motion correction with targeted-PROPELLER. Full FOV PROPELLER data that included both the moving and static objects were first acquired with images reconstructed both with and without motion correction. Next, 1/2 FOV targeted-PROPELLER data were acquired with the targeted FOV specifically positioned to encompass the continuously moving object. A second targeted PROPELLER acquisition was performed with targeted FOV encompassing the static object. Again, targeted-PROPELLER images were reconstructed with and without motion correction. Imaging parameters were FOV = 200 × 200/100 × 100 mm^2 (full FOV/targeted FOV), TH = 5 mm, TR/TE = 2500/56 ms, matrix = 128 × 128.

Volunteer Studies

Study protocols were approved by our Institutional Review Board and written informed consent was obtained from each volunteer. We sought to qualitatively demonstrate the feasibility of using the proposed targeted-PROPELLER methods for a wide range of imaging applications. In 5 normal volunteer studies, we acquired both conventional and targeted-PROPELLER images for either brain, abdominal, vessel wall, or cardiac applications. A detailed list of the imaging parameters used for these studies is included in Table 1.

Brain

Axial and coronal brain images across the lateral ventricle were acquired using a 4-channel head coil. Full FOV PROPELLER and 1/2 FOV targeted-PROPELLER images were acquired with and without DEFT to demonstrate the recovery of signal at the end of each TR because of the long T1 and T2 values in the brain tissues (Table 1, brain). Next, we acquired 1/2 and 1/4 FOV targeted-PROPELLER images with the same spatial resolution (0.8 × 0.8 mm^2) as the full FOV PROPELLER images but requiring less imaging time (Table 1, targeted-PROPELLER brain study 1). Additionally, a 1/2 FOV targeted-PROPELLER image with improved spatial resolution (0.4 × 0.4 mm^2) was acquired without increasing imaging time compared with the full FOV PROPELLER image (Table 1, targeted-PROPELLER brain study 2).

Abdomen

Abdominal images were acquired using anterior surface coils and posterior spine array coils. Full FOV PROPELLER and 1/2 FOV targeted-PROPELLER abdominal images that included the left kidney were acquired in the sagittal orientation (Table 1, abdomen). Abdominal imaging was performed during free-breathing with no synchronization between MR data acquisition and the volunteer's respiratory cycle. The purpose of this portion of the study was to demonstrate the differential impact of targeted acquisition methods on the efficacy of in vivo motion correction. The selected sagittal imaging plane contained kidney and abdominal wall, each with different patterns of motion during the respiratory cycle. Full FOV PROPELLER and 1/2 FOV targeted-PROPELLER images were reconstructed with self-navigated motion correction. Full FOV PROPELLER and targeted-PROPELLER images were also reconstructed from undersampled *k*-space datasets (ie, reducing Nblade) to demonstrate differential motion impact when reducing the overall imaging time.

Cardiac

ECG-gated T2W dark-blood images in the short-axis orientation were acquired using conventional full FOV PROPELLER and HASTE approaches. Additionally, reduced FOV dark-blood targeted- PROPELLER and targeted-HASTE images were acquired with FOV limited to complete coverage of the cardiac chambers. PROPELLER imaging parameters are listed in Table 1, cardiac. Imaging parameters for HASTE sequences (full FOV/targeted FOV) were: FOV = 226 × 350/115 × 115, imaging matrix = 124 × 192/64 × 64, ETL = 78/48, BW = 798 Hz/pixel. TR = 2 × R-R interval, TE = 62 ms, TH = 5mm. Acquisition time was roughly was 2 seconds for both full FOV HASTE and targeted-HASTE, and 12 second for targeted-HASTE with 6 signal averages. All cardiac sequences used a double-inversion recovery pulse for dark-blood preparation with an inversion time of 1000 ms. Breath-holds were requested during imaging and no motion correction was performed. A parallel imaging technique, generalized auto-calibrating partially parallel acquisitions (GRAPPA)[24] with acceleration rate = 2 was required to acquire full FOV PROPELLER images within a 20-second breath-hold.

Vessel Wall

T2W dark-blood vessel wall images within the abdominal descending aorta were acquired in the transverse plane using the conventional full FOV PROPELLER and targeted-PROPELLER sequences with imaging parameters listed in Table 1, vessel wall. A double-inversion recovery pulse for dark-blood imaging with inversion time of 1000 ms was used. Breath-holds were requested during imaging and no motion correction was performed. For targeted-PROPELLER, the FOV was tapered from 1/3 to 1/6 of the full FOV targeting the cross-sectional area of the aorta. For a 1/6 FOV targeted-PROPELLER image acquired with higher spatial resolution, *k*-space oversampling (ie, 300% blade coverage for data averaging) was used to improve SNR.

RESULTS

Phantom Studies

The full FOV PROPELLER resolution phantom image is shown in Figure 2A. Both targeted-HASTE and targeted-PROPELLER approaches were able to limit the FOV to a small region centered on the resolution markers within the upper left quadrant of the phantom. For both approaches IVI methods permitted a reduced FOV whereas avoiding wrapping artifacts. Targeted-HASTE (Figs. 2B and C) and single blade (N_{blade} = 1, ETL = 128) targeted-PROPELLER (Fig. 2D) images were blurred along the PE direction, because of T2W filtering effects. However, targeted-PROPELLER images reconstructed from the oversampled *k*-space covered with overlapping concentric blades (N_{blade} = 2, 4, 8, ETL = 128) demonstrated isotropic spatial resolution with less image blurring (Figs. 2E–G). A striking improvement was clearly evident with the inclusion of only a single additional *k*-space blade (Fig. 2E).

For the motion phantom study, a full FOV image acquired at stationary phantom status (Fig. 3A) shows the dynamic object sitting atop the balloon filled with both water and air; static object is position at right. Full FOV PROPELLER images and targeted-PROPELLER images were acquired during the continuous inflation/deflation of the balloon. Full FOV PROPELLER image without motion correction (Fig. 3B) demonstrated blurring of the moving object along the motion trajectory without blurring of the static object. The motion-corrected full FOV PROPELLER image (Fig. 3C) partially restored the shape and original position of the moving object (Fig. 3D) but blurred and distorted both the moving and static objects (Figs. 3D and E). However, the motion was more effectively corrected within the 1/2 FOV targeted-PROPELLER images that specifically targeted the moving object (Figs. 3F and zoom-in 3G). Motion of the dynamic object had no apparent impact on static object image separately acquired with FOV targeted to the static object (Fig. 3H).

Volunteer Studies

Brain—Full FOV and 1/2 FOV targeted-PROPELLER images with and without DEFT were shown in Figure 4A. Images acquired with DEFT (Figs. 4A, D–F) provided greater overall signal intensity and superior image contrast between the cerebrospinal fluid within the lateral ventricles and brain tissues, compared with those acquired without DEFT (Figs. 4A–C). Targeted-PROPELLER images (Figs. 4A, C and Figs. 4A, F), with identical voxel size but requiring 1/2 acquisition time, provided similar image contrast as full FOV images (Figs. 4A, B and Figs. 4A, E), and there were no apparent wrapping artifacts. However, as expected, SNR was appreciably lower within targeted-PROPELLER images because of the reduced matrix size.

Compared with full FOV PROPELLER images (Figs. 4A, B), targeted-PROPELLER images with 1/2 FOV (Figs. 4B, D) and 1/4 FOV (Figs. 4B, E) achieved similar relative image quality and spatial resolution whereas requiring 1/2 and 1/4 acquisition times, respectively. Also, higher spatial resolution for a 1/2 FOV targeted-PROPELLER image (Figs. 4B, F) was achieved without increasing acquisition time compared with the full FOV image at lower resolution. The latter examples demonstrated the potential to use targeted-PROPELLER techniques to selectively interrogate a small ROI with increased spatial resolution but only minimal penalties in imaging time.

Abdominal Imaging—Motion-corrected full FOV PROPELLER images containing kidney and abdominal wall (Fig. 5A) demonstrated a blurred profile of the kidney with streak artifacts. Motion-corrected targeted-PROPELLER images with 1/2 FOV encompassing the left kidney (Fig. 5C) better delineated the kidney anatomy with less blurring and streak artifacts compared with the full FOV PROPELLER images. Increased spatial resolution for a 1/2 FOV targeted-PROPELLER image (Fig. 5D) was achieved without increasing acquisition time compared with the full FOV image whereas also avoiding motion artifacts. Signal intensity within renal artery and renal vein at the renal hilus was hyperintense in full FOV PROPELLER images but suppressed in targeted-PROPELLER images. Spins of the blood outside of the targeted imaging FOV experiencing excitation pulse resulted in spin dephasing and thus the saturation of blood signals in the targeted-PROPELLER images.

Full FOV PROPELLER images reconstructed with *k*-space undersampling (Figs 5E and H) demonstrated downgraded image quality with increased motion artifacts and steak artifacts compared with images reconstructed from fully sampled *k*-space. However, targeted-PROPELLER images were less sensitive to *k*-space under-sampling with image blurring but no obvious motion artifacts (Fig. 5G and J). Overall, targeted-PROPELLER provided more robust regional motion correction compared with full FOV PROPELLER images.

Cardiac—Full FOV PROPELLER and HASTE images along with 1/3 FOV targeted-HASTE and targeted-PROPELLER images in the cardiac short-axis orientation are shown in Figure 6. The full FOV HASTE image was blurred along the A-P orientation because of fast T2 decay of the myocardium (Fig. 6A). Targeted-HASTE images reduced blurring by reducing the single-shot ETL (Figs. 6E and F [6 averages]). A full FOV PROPELLER image (Fig. 6C), acquired with GRAPPA to reduce acquisition time to within a 20-s breath-hold, provided isotropic spatial resolution qualitatively sharper than anisotropic HASTE approaches. A corresponding targeted-PROPELLER image (Fig. 6G), without GRAPPA, was acquired within a 12-s breath-hold. A 60% *k*-space undersampled targeted-PROPELLER acquisition provided similar image quality within a reduced 8s breathhold (Fig. 6H). *K*-space undersampling resulted in imaging blurring compared with the fully sampled targeted-PROPELLER image but most anatomic structures within the heart continued to be clearly delineated. A high-resolution targeted-PROPELLER image, acquired using a reduced voxel

size but still within a ~20-s breathhold, provided superior anatomic delineation of fine cardiac structures with particularly fine depiction of the papillary muscles and trabecula (Fig. 6I).

Vessel Wall—Full FOV PROPELLER (Fig. 7A) and 1/3 FOV targeted-PROPELLER (Fig. 7C) images were acquired at a cross-sectional position within descending aorta in the lower abdomen (1.8×1.8 mm^2). 1/3 FOV targeted-PROPELLER images provided similar depiction of the aortic vessel wall but required 1/3 the acquisition time of the corresponding full FOV image. A 1/6 FOV targeted-PROPELLER image (Fig. 7E) acquired with higher spatial resolution (1.0×1.0 mm^2) improved image quality providing superior delineation of lumen and the vessel wall. Vessel wall was sharply delineated with blood signal within the lumen effectively suppressed in the targeted-PROPELLER images.

DISCUSSION

In these initial phantom and normal volunteer studies, we demonstrated the feasibility of using targeted-PROPELLER approaches to limit the imaging FOV thereby reducing acquisition times or permitting increased spatial resolution without commensurate increases in scan time. Compared with previous targeted-HASTE approaches, targeted-PROPELLER permits a flexible tradeoff between desired isotropic spatial resolution and overall acquisition time that can be tailored to a specific application. We demonstrated the potential efficacy of this new technique in brain, abdominal, cardiac, and vessel wall imaging studies. Both phantom and in vivo motion studies demonstrated the potential for more robust regional self-navigated motion correction compared with conventional full FOV PROPELLER methods.

PROPELLER techniques have been successfully employed for brain and body imaging applications to provide superior image quality with less sensitivity to field inhomogeneities and reduced motion artifacts.[1–4,6,7,9–11,25] Our study combined the inner volume excitation technique with conventional PROPELLER to acquire signals from a selected volume whereas avoiding signals outside of the ROI. With targeted-PROPELLER, a reduced imaging matrix size reduced the number of blades and therefore reduced imaging time. Additionally, targeted-PROPELLER provided a method of improving the spatial resolution in a small ROI without penalties in imaging time compared with the corresponding full FOV images.

Targeted-HASTE techniques have previously been used during MR-guided interventional procedures to accelerate real-time image acquisition rates and reduce blurring of biopsy needles.[18,19] However, with this approach image blurring along the PE direction may still occur in objects with short T2. In our first phantom study, targeted-HASTE images (effectively ETL = 68, for partial-Fourier acquisition of 128 matrix) showed blurring between resolution grids along PE directions because of T2 decay. The targeted-PROPELLER images (even with fully sampled matrix, ETL = 128) mitigated these blurring effects providing isotropic spatial resolution by sampling rotated and overlapping data segments along angularly variant PE directions (ie, the *k*-space blades). These findings suggest that targeted-PROPELLER has the potential to serve as a complementary method for MR-guided interventional procedures with the number of data segments adjusted to achieve a balance between improved image sharpness and imaging time. Therefore, targeted-PROPELLER techniques may provide a promising alternative during MR-guided interventions for better needle visualization.

PROPELLER uses a self-navigated method for translational and rotational motion correction based on the oversampled central circle region in each individual blade *k*-space dataset. For cardiac motions with a complex pattern distinct from motions of chest wall and other organs present in the imaging volume, previous studies proposed a modified regional motion correction algorithm.[1] Motion estimation was performed based on tapered blade images of a smaller region, and the estimated motion from this region was removed from the original,

unmasked data for the final reconstruction. In targeted-PROPELLER, regional motion correction within a limited FOV, targeting only the moving object, resulted in improved motion correction. Our motion phantom study and in vivo abdominal motion studies demonstrated that targeted-PROPELLER may be able to provide more robust regional self-navigated motion correction compared with the full FOV PROPELLER images in the presence of multiple motion patterns within the FOV. Particularly for in vivo abdominal imaging, this improvement became more dramatic when comparing full FOV PROPELLER and targeted-PROPELLER images reconstructed from undersampled *k*-space datasets. We suspect that this finding may be because of reduced low-spatial frequency averaging for these undersampled datasets leading to reduced mitigation of remnant motion artifacts in the full FOV PROPELLER images. Regional motion correction with targeted-PROPELLER may offer an attractive approach for cardiac imaging during free-breathing or potentially fetal imaging with in utero motion patterns independent from the mother's bulk motions.

Targeted-PROPELLER approaches have several limitations that are inherent to most IVI methods.[16] Targeted-PROPELLER offers to improve imaging efficiency at the expense of in-plane spatial coverage. Such a trade-off may only be appropriate when prior knowledge of an appropriate targeted ROI is made available by some alternate means. However, one could conceivably use targeted-PROPELLER methods to provide high-resolution images of a specific ROI, targeting smaller anatomic structures such as vessel wall[26] and myocardium[27] to assess these pathologies with accelerated imaging time. Targeted-PROPELLER methods could also be combined with magnetization preparation schemes (T2, T1, diffusion, perfusion) for more rapid quantitative measurements within specific ROI as demonstrated with previous 2D ss-rFOV-DWEPI[20] and 3D ss-DWSTEPI[21] methods. Additionally, IVI approaches inherently suffer from reduced SNR compared with full FOV image acquisition.[16] Further studies may be necessary to optimally tailor targeted-PROPELLER image acquisition time, signal averaging, and spatial resolution for specific imaging applications. Finally, the altered orientation of section-selective gradients during 90° excitation will complicate multislice image acquisition. Depending on the chosen excitation flip-angle and tissue T1, interleaved slice acquisition to accelerate volumetric coverage may not be feasible because of insufficient magnetization recovery time between excitations. However, the perpendicular orientation of section-selective gradients for 90° excitation and subsequent 180° refocusing RF pulses could also be advantageous providing an alternative means to saturate inflowing blood signals to improve contrast between lumen and surrounding tissues during cardiac or vessel wall imaging.

This initial feasibility study described the methodology and utility of the targeted-PROPELLER imaging technique for different applications in a limited number of volunteer studies. Relative image quality (eg, spatial resolution, imaging artifacts) was qualitatively assessed with comparisons to conventional PROPELLER methods and previously developed targeted-HASTE techniques. Future studies are necessary to validate these targeted-PROPELLER techniques in a series of clinical patient studies. For each application, rigorous quantitative comparisons to standard clinical protocols will be necessary to fully evaluate trade-offs between acquisition time, SNR, CNR, and image artifact levels and even more importantly the reproducible efficacy of these methods for providing accurate clinical diagnoses.

In conclusion, these descriptive studies have demonstrated that targeted-PROPELLER is a promising technique to (*a*) reduce imaging time or (*b*) improve spatial resolution with minimal penalties on overall acquisition time. Targeted-PROPELLER additionally offers the potential for more effective regional motion correction to produce images otherwise corrupted with remnant uncorrected image artifacts because of a range of different motion patterns within the larger image volume.

References

1. Pipe JG. Motion correction with PROPELLER MRI: application to head motion and free-breathing cardiac imaging. Magn Reson Med 1999;42:963–969. [PubMed: 10542356]
2. Wintersperger BJ, Runge VM, Biswas J, et al. Brain magnetic resonance imaging at 3 Tesla using BLADE compared with standard rectilinear data sampling. Invest Radiol 2006;41:586 –592. [PubMed: 16772852]
3. Forbes KP, Pipe JG, Karis JP, et al. Brain imaging in the unsedated pediatric patient: comparison of periodically rotated overlapping parallel lines with enhanced reconstruction and single-shot fast spin-echo sequences. AJNR Am J Neuroradiol 2003;24:794 –798. [PubMed: 12748073]
4. Naganawa S, Satake H, Iwano S, et al. Contrast-enhanced MR imaging of the brain using T1-weighted FLAIR with BLADE compared with a conventional spin-echo sequence. Eur Radiol 2008;18:337–342. [PubMed: 17922279]
5. Attenberger UI, Runge VM, Williams KD, et al. T1-Weighted brain imaging with a 32-channel coil at 3T using TurboFLASH BLADE compared with standard cartesian k-space sampling. Invest Radiol 2009;44:177–183. [PubMed: 19151605]
6. Pipe JG, Farthing VG, Forbes KP. Multishot diffusion-weighted FSE using PROPELLER MRI. Magn Reson Med 2002;47:42–52. [PubMed: 11754441]
7. Deng J, Miller FH, Salem R, et al. Multishot diffusion-weighted PROPELLER magnetic resonance imaging of the abdomen. Invest Radiol 2006;41:769–775. [PubMed: 16971801]
8. Deng J, Omary RA, Larson AC. Multishot diffusion-weighted SPLICE PROPELLER MRI of the abdomen. Magn Reson Med 2008;59:947–953. [PubMed: 18429036]
9. Kabasawa H, Masutani Y, Aoki S, et al. 3T PROPELLER diffusion tensor fiber tractography: a feasibility study for cranial nerve fiber tracking. Radiat Med 2007;25:462– 466. [PubMed: 18026904]
10. Adachi M, Kabasawa H, Kawaguchi E. Depiction of the cranial nerves within the brain stem with use of PROPELLER multishot diffusion-weighted imaging. AJNR Am J Neuroradiol 2008;29:911–912. [PubMed: 18258705]
11. Forbes KP, Pipe JG, Karis JP, et al. Improved image quality and detection of acute cerebral infarction with PROPELLER diffusion-weighted MR imaging. Radiology 2002;225:551–555. [PubMed: 12409594]
12. Larson PE, Nishimura DG. Anisotropic field-of-views for PROPELLER MRI. Proc Intl Soc Mag Reson Med 2007;15:1726.
13. Devaraj A, Pipe JG. Elliptical field of view in PROPELLER MRI. Proc Intl Soc Mag Reson Med 2007;15:1665.
14. Arfanakis K, Tamhane AA, Pipe JG, et al. k-space undersampling in PROPELLER imaging. Magn Reson Med 2005;53:675– 683. [PubMed: 15723398]
15. Pipe JG, Zwart N. Turboprop: improved PROPELLER imaging. Magn Reson Med 2006;55:380 –385. [PubMed: 16402378]
16. Feinberg DA, Hoenninger JC, Crooks LE, et al. Inner volume MR imaging: technical concepts and their application. Radiology 1985;156:743–747. [PubMed: 4023236]
17. Makki M, Graves MJ, Lomas DJ. Interactive body magnetic resonance fluoroscopy using modified single-shot half-Fourier rapid acquisition with relaxation enhancement (RARE) with multiparameter control. J Magn Reson Imaging 2002;16:85–93. [PubMed: 12112507]
18. Zimmermann H, Muller S, Gutmann B, et al. Targeted-HASTE imaging with automated device tracking for MR-guided needle interventions in closed-bore MR systems. Magn Reson Med 2006;56:481– 488. [PubMed: 16795081]
19. Buecker A, Adam G, Neuerburg JM, et al. MR-guided biopsy using a T2-weighted single-shot zoom imaging sequence (Local Look technique). J Magn Reson Imaging 1998;8:955–959. [PubMed: 9702898]
20. Jeong EK, Kim SE, Guo J, et al. High-resolution DTI with 2D interleaved multislice reduced FOV single-shot diffusion-weighted EPI (2D ss-rFOV-DWEPI). Magn Reson Med 2005;54:1575–1579. [PubMed: 16254946]

21. Jeong EK, Kim SE, Kholmovski EG, et al. High-resolution DTI of a localized volume using 3D single-shot diffusion-weighted STimulated echo-planar imaging (3D ss-DWSTEPI). Magn Reson Med 2006;56:1173–1181. [PubMed: 17089367]

22. Becker ED, Farrar TC. Driven equilibrium Fourier transform spectroscopy. A new method for nuclear magnetic resonance signal enhancement. J Am Chem Soc 1969;91:7784 –7785. [PubMed: 5357869]

23. Busse RF, Riederer SJ, Fletcher JG, et al. Interactive fast spin-echo imaging. Magn Reson Med 2000;44:339 –348. [PubMed: 10975883]

24. Griswold MA, Jakob PM, Heidemann RM, et al. Generalized autocalibrating partially parallel acquisitions (GRAPPA). Magn Reson Med 2002;47:1202–1210. [PubMed: 12111967]

25. Mori H, Aoki S, Abe O, et al. Evaluation of PROPELLER MR imaging: preliminary experiences. Nippon Igaku Hoshasen Gakkai Zasshi 2002;62:287–289. [PubMed: 12073636]

26. Maroules CD, McColl R, Khera A, et al. Assessment and reproducibility of aortic atherosclerosis magnetic resonance imaging: impact of 3-Tesla field strength and parallel imaging. Invest Radiol 2008;43:656–662. [PubMed: 18708860]

27. Tilak GS, Hsu LY, Hoyt RF Jr, et al. In vivo T2-weighted magnetic resonance imaging can accurately determine the ischemic area at risk for 2-day-old nonreperfused myocardial infarction. Invest Radiol 2008;43:7–15. [PubMed: 18097272]

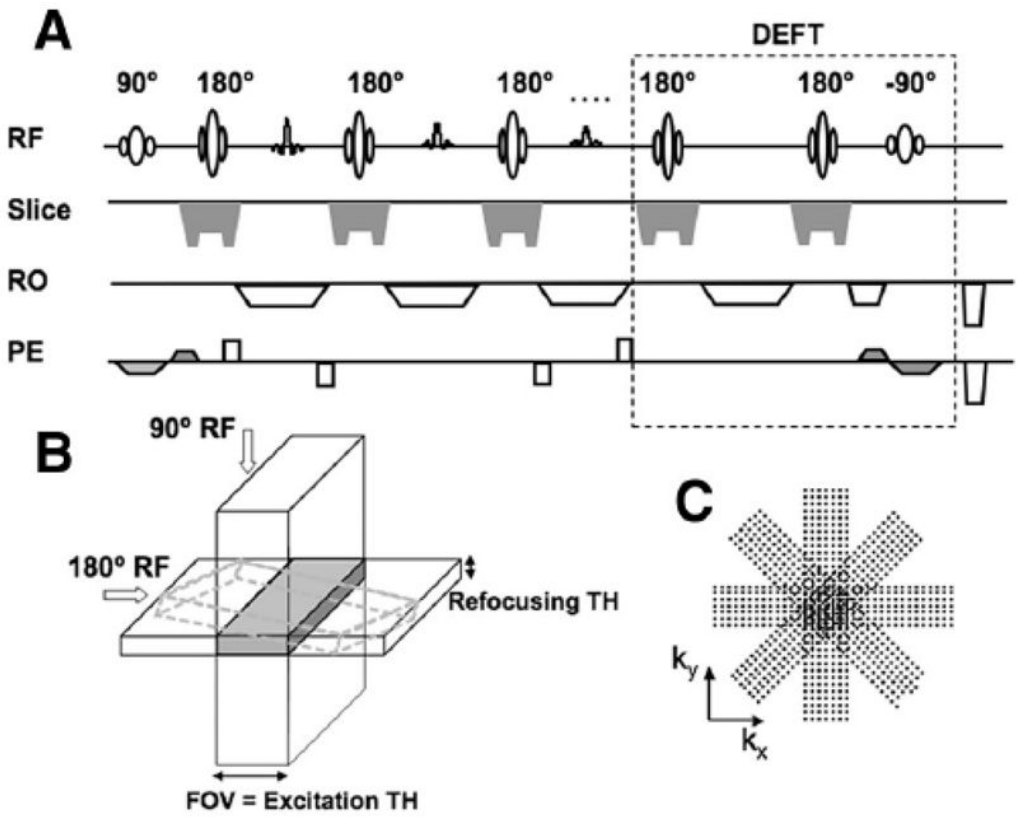

FIGURE 1.

Diagram of the modified PROPELLER sequence depicting a single representative *k*-space blade acquisition. The sequence diagram (A) and slice selection illustration (B) demonstrated that slice selection gradient of the excitation RF pulse was applied along PE direction, perpendicular to that of the refocusing RF pulse to provide limited FOV along the PE direction. At the end of each echo train, DEFT technique (dashed box) using a −90° RF pulse with slice selection gradients along the PE direction was applied to flip the residual transverse magnetization back to the longitudinal axis. C, PROPELLER *k*-space trajectory with concentric and rectilinear data segments rotating around the central *k*-space. RF indicates radio frequency pulse; RO, readout; PE, phase-encoding; TH, slice thickness; DEFT, driven-equilibrium Fourier transform.

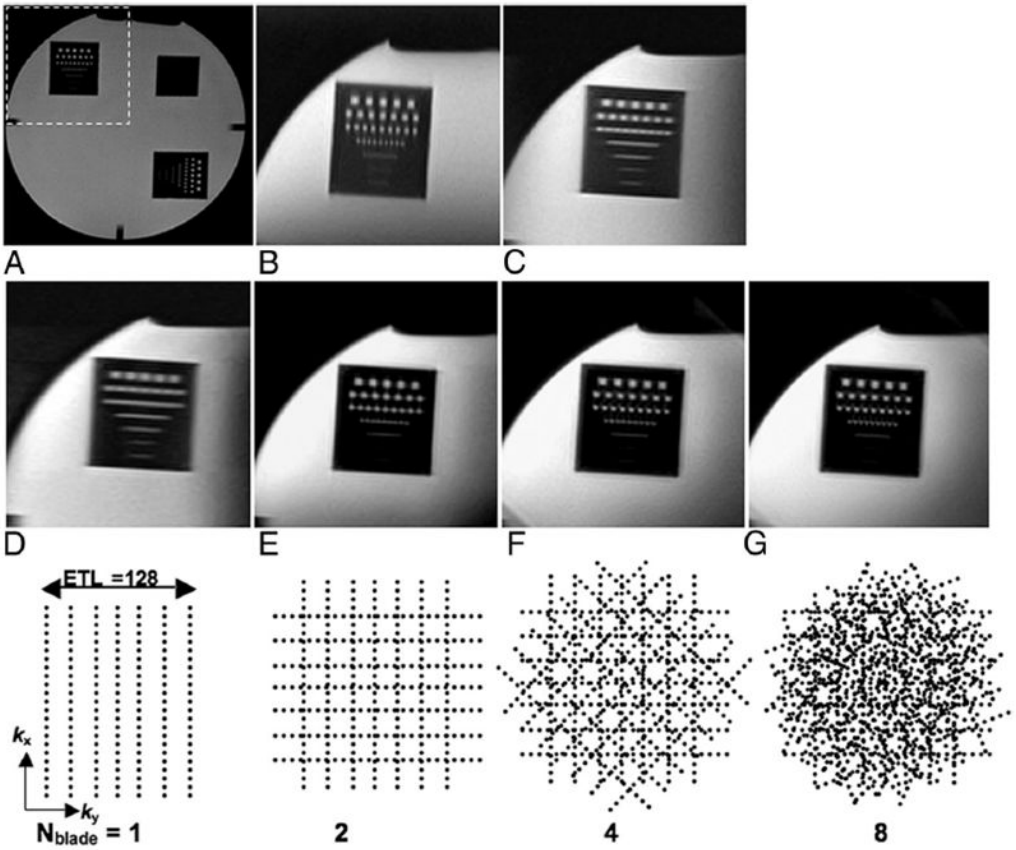

FIGURE 2.

Full FOV PROPELLER image of resolution phantom (A) and 1/2 FOV phantom images (B–G) centered on the resolution markers within the upper left quadrant of the phantom (dashed box in A). Half FOV targeted-HASTE images with PE along AP (B) and LR directions (C). A 1/2 FOV single-blade targeted-PROPELLER image acquired with LR PE direction and N_{blade} = 1, blade width = ETL = 128 (D). Half FOV targeted-PROPELLER images reconstructed from oversampled PROPELLER *k*-space datasets with an increasing number of blades (N_{blade} = 2, 4, and 8) (E–G). Corresponding *k*-space sampling patterns for each targeted-PROPELLER image (D–G) are shown along the bottom row. Notice blurring of the resolution markers along the PE directions in B, C, and D along with the superior isotropic spatial resolution provided in E, F, and G.

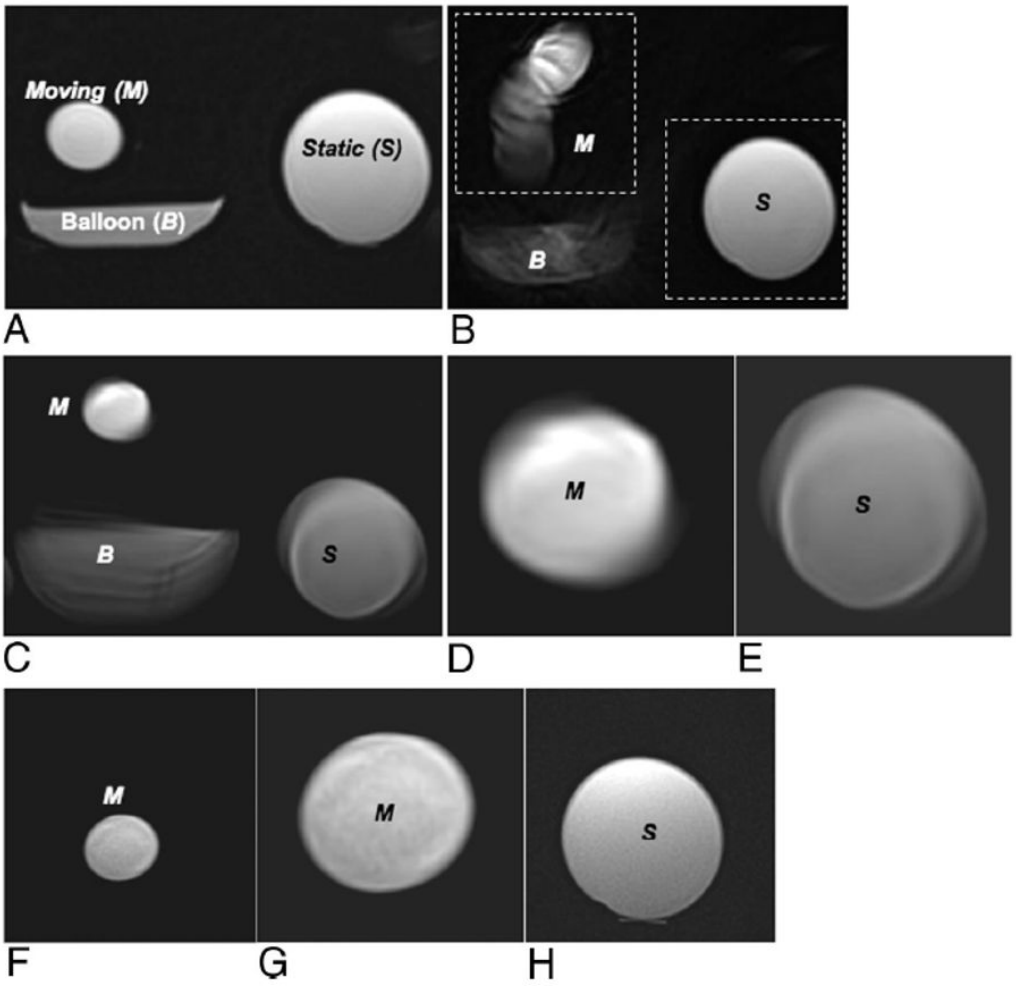

FIGURE 3.

Phantom model consisting of a static object and a moving object sitting atop a balloon that was inflated and deflated with water. Full FOV PROPELLER image during stationary conditions (A) compared with full FOV PROPELLER image during object motion without (B) and with self-navigated motion correction (C). Inset magnified images demonstrate distortion and blurring of both moving (D) and static objects (E) within the motion-corrected full FOV images. Motion-corrected 1/2 FOV (dashed box in B) targeted-PROPELLER images separately targeting the moving (F, with same FOV magnified in G) and static (H) objects. Notice that moving and static objects were both blurred and distorted in the motion-corrected full FOV image (C–E), whereas motion of the moving object was effectively corrected in 1/2 FOV targeted-PROPELLER image targeting the moving object (F, G) with no impact on the static object image (H).

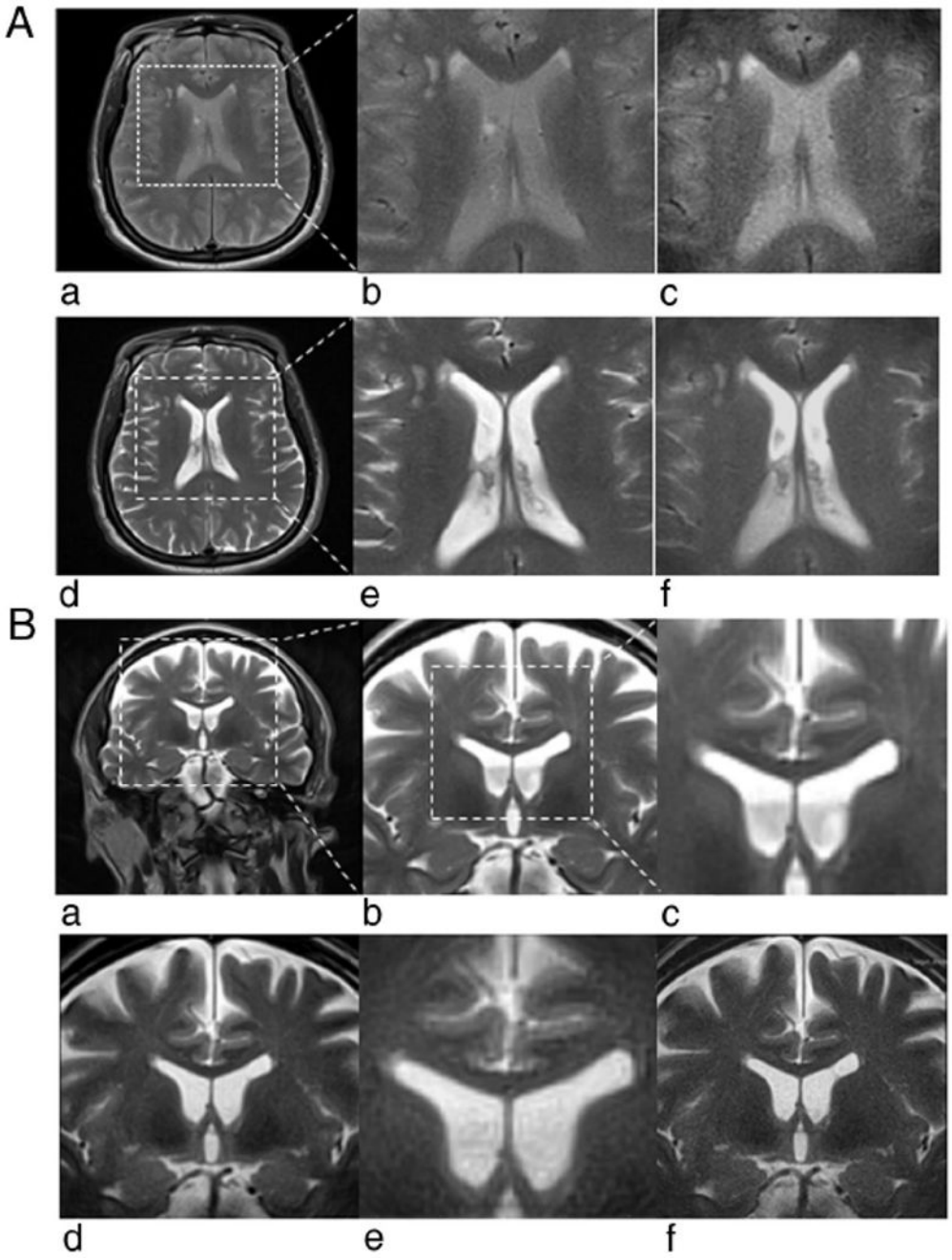

FIGURE 4.

A, Full FOV and 1/2 FOV PROPELLER brain images acquired without DEFT (a– c) and with DEFT (d–f). Full FOV (a) and inset from full FOV (×2) (b) PROPELLER images along with 1/2 FOV targeted-PROPELLER images (c) of the brain without DEFT showed reduced overall signal intensity and limited contrast between anatomic structures compared with those full FOV PROPELLER (d and e) and targeted-PROPELLER (f) images with DEFT. B, Full FOV (a) and insets from full FOV (×2 and ×4) (b and c) PROPELLER images of the brain compared with 1/2 FOV (d) and 1/4 FOV (e) targeted-PROPELLER images all with identical voxel sizes (0.8×0.8 mm^2) but (d) and (e) requiring 1/2 and 1/4 the acquisition time of full FOV image

(a). Half FOV targeted-PROPELLER image (f) with decreased voxel size (0.4×0.4 mm^2) but same acquisition time as full FOV image (a).

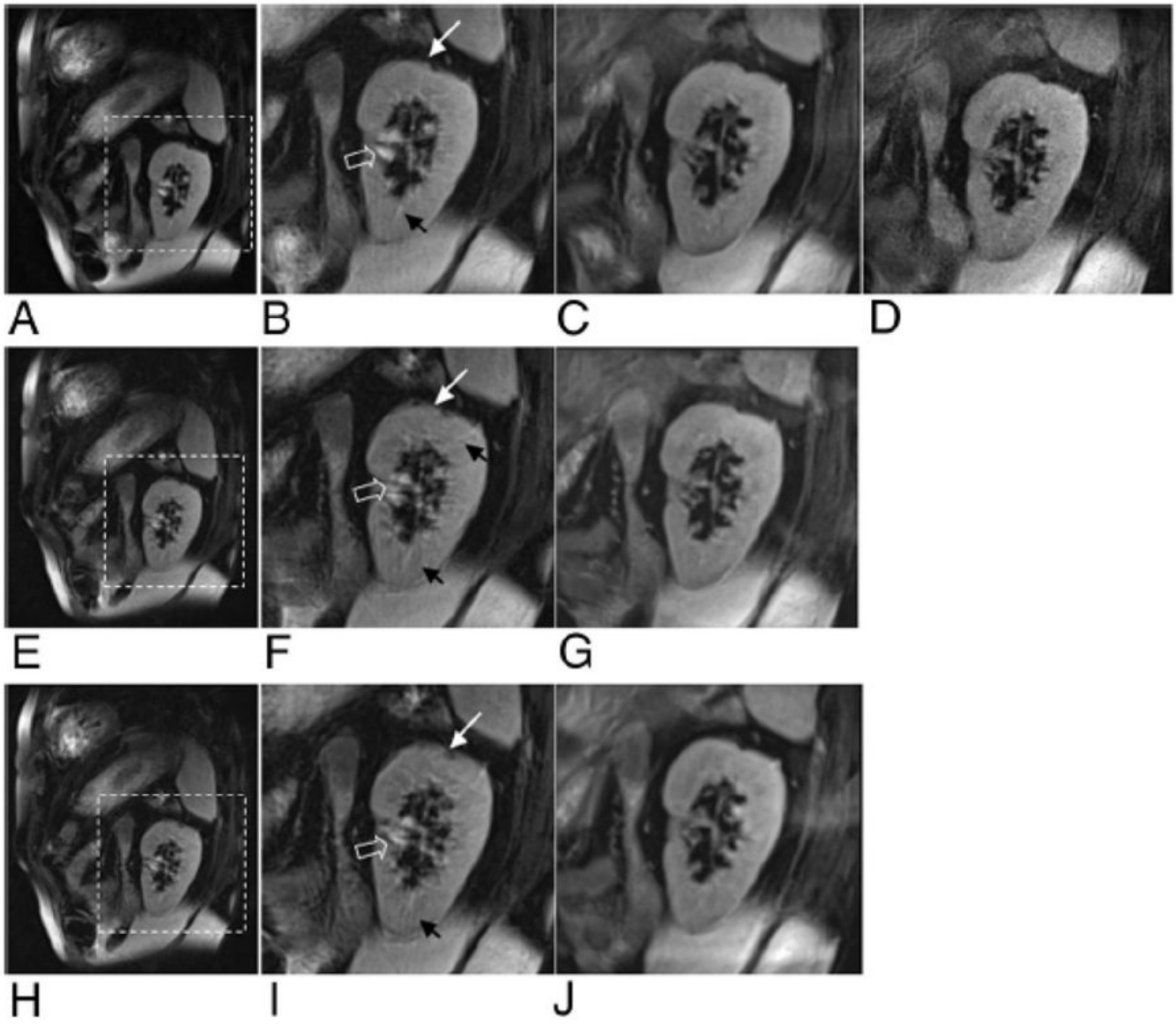

FIGURE 5.

Full FOV PROPELLER and targeted-PROPELLER images acquired during free breathing reconstructed with self-navigated motion correction. Full FOV (A) and insets from full FOV (×2) (B) PROPELLER images of the left kidney compared with 1/2 FOV (C, D) targeted-PROPELLER images with identical voxel size (1.2 × 1.2 mm^2) and decreased voxel size (0.8 × 0.8 mm^2). Full FOV (E and H) and insets from full FOV (×2) (F and I) PROPELLER images datasets compared with 1/2 FOV (G and J) targeted-PROPELLER images reconstructed from 25% and 50% undersampled *k*-space datasets, respectively, each with identical voxel size (1.2 × 1.2 mm^2). Notice that full FOV PROPELLER images (A–B, E–F, and H–I) demonstrated image blurring and streak artifacts because of motion (solid arrows) compared with reduced FOV targeted-PROPELLER images (C, D, G, and J). Blood signal at renal hilus was hyperintense in full FOV images (hollow arrows) but suppressed in targeted-PROPELLER images because of perpendicular spatial orientations of IVI excitation and refocusing pulses.

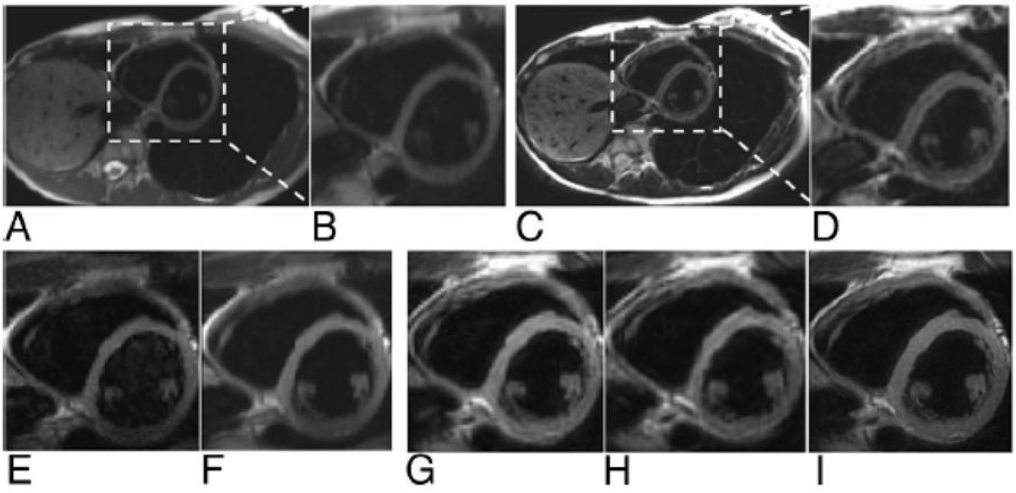

FIGURE 6.

Dark blood cardiac images acquired in short-axis orientation with HASTE (A with ×3 inset shown in B) and full FOV PROPELLER (C with ×3 inset shown in D) along with corresponding 1/3 FOV targeted-HASTE images (E and F with 6 averages) and targeted-PROPELLER (G, H with 60% *k*-space undersampling, and I with increased spatial resolution). Notice the blurring of HASTE images along the A-P PE direction, which is reduced with targeted-HASTE acquisition but inferior to isotropic resolution provided with PROPELLER approaches. Notice the superior depiction of fine anatomic structures within high resolution targeted-PROPELLER image (I) acquired within a single breath-hold.

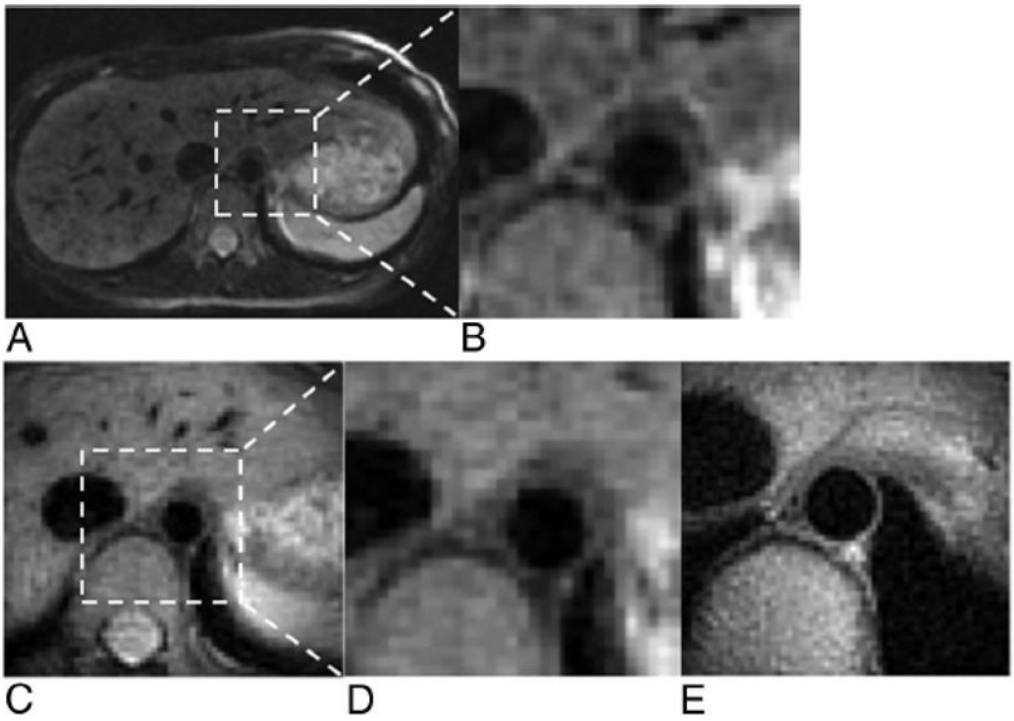

FIGURE 7.

Dark-blood vessel wall imaging of the descending aorta. Full FOV PROPELLER (A) and ×6 inset (B) images were comparable with corresponding 1/3 FOV targeted-PROPELLER (C) and ×2 inset (D) images that required a 12 seconds acquisition. A 1/6 FOV targeted-PROPELLER image (E) targeting cross-sectional region of the aorta provided improved spatial resolution for superior delineation of the vessel wall and lumen.

TABLE 1

Imaging Parameters for Conventional Full FOV PROPELLER and Reduced FOV Targeted-PROPELLER Images for In Vivo Applications

	Brain		**Abdomen**		**Cardiu**	**Vessel Wall**
Full FOV PROPELLER						
FOV (mm^2)	200 × 200		300 × 300		350 × 350	350 × 350
TR (ms)	2000		3000		2 × R-R	2 × R-R
TE (ms)	100		90		58	58
TH (mm)	5		5		5	3
Matrix	256		256		192	192
Resolution (mm^2)	0.8 × 0.8		1.2 × 1.2		1.8 × 1.8	1.8 × 1.8
ETL	25		28		21	21
Blade coverage (BC) (%)	100	100	73.3	53.3	100	100
N_{blade} × BC	17	15	11	8	9	9
BW (Hz/Pi)	400		400		235	235
TA (min:sec)	0:36	0:48	0:36	0:27	0:20	0:20
GRAPPA	No		No		Yes	Yes
Others	DEFT vs. no DEFT		Fat saturation		DIR	DIR
			Free breathing		ECG gating	Fat saturation
			Motion correction			ECG gating

	Brain 1		**Brain 2**		**Abdomen**				**Cardiac**		**Vessel Wall**	
Targeted-PROPELLER												
FOV (mm^2)	100 × 100	50 × 50	100 × 100		150 × 150				115 × 115		115 × 115	66 × 66
TR (ms)	2000		2000		3000				2 × R-R		2 × R-R	
TE (ms)	100		100		90				58		58	
TH (mm)	5		5		5				5		3	
Matrix	128	64	256		128		192	64			64	
Resolution (mm^2)	0.8 × 0.8		0.4 × 0.4		1.2 × 1.2		0.8 × 0.8	1.8 × 1.8	0.9 × 0.9	128	1.8 × 1.8	1.0 × 1.0
ETL	25		25		28				21		21	
Blade coverage (BC) (%)	100		100	100	75	50	100	100	60	100	100	300
N_{blade} × BC	9	5	17	8	6	4	12	5	3	10	5	15
BW (Hz/Px)	400		400		400				235		235	

	Brain				Abdomen			Cardiu		Vessel Wall	
TA (min:sec)	0:20	0:12	0:36	0:27	0:21	0:15	0:39	0:12	0:08	0:22	0:12	0:32
Others	DEFT vs. no DEFT		DEFT		Fat saturation				DIR		DIR	
					Free breathing				ECG gating		Fat saturation	
					Motion correction						ECG gating	